Chemical Engineering Journal 456 (2023) 140807

Contents lists available at ScienceDirect

Chemical Engineering Journal

journal homepage: www.elsevier.com/locate/cej

Constructing efficient CuO_x-CeO_2 catalyst for NO reduction by CO: New insights into the structure–activity relationship

Wei Tan [a,b,1], Yandi Cai [a,1], Shaohua Xie [b], Juntian Xu [a], Kaili Ma [c], Kailong Ye [b], Lu Ma [d], Steven N. Ehrlich [d], Weixin Zou [a], Fei Gao [a,*], Lin Dong [a], Fudong Liu [b,*]

[a] State Key Laboratory of Pollution Control and Resource Reuse, School of Environment, Jiangsu Key Laboratory of Vehicle Emissions Control, Center of Modern Analysis, Key Laboratory of Mesoscopic Chemistry of MOE, School of Chemistry and Chemical Engineering, Nanjing University, Nanjing 210023, China
[b] Department of Civil, Environmental, and Construction Engineering, Catalysis Cluster for Renewable Energy and Chemical Transformations (REACT), NanoScience Technology Center (NSTC), University of Central Florida, Orlando, FL 32816, United States
[c] Analysis and Testing Center, Southeast University, Nanjing 211189, China
[d] National Synchrotron Light Source II (NSLS-II), Brookhaven National Laboratory, Upton, NY 11973, United States

ARTICLE INFO

Keywords:
NO reduction by CO
highly dispersed CuO-CeO_2
Redox property
Oxygen vacancy
NO dissociation

ABSTRACT

CuO-CeO_2 based materials have been recognized as promising substitutes for precious metal catalysts in emission control field due to their superior redox property and low cost. Herein, by optimizing the deposition process of CeO_2 and CuO onto γ-Al_2O_3, highly dispersed CuO clusters on unique CeO_2-Al_2O_3 support with small CeO_2 particles (7Cu-Ce/CeAl) were successfully constructed for efficient NO reduction by CO, which exhibited much higher NO removal efficiency and N_2 selectivity than CuO catalysts supported on γ-Al_2O_3 (7Cu/Al) and conventional CeO_2-Al_2O_3 support (7Cu/CeAl). Moreover, H_2O showed limited inhibition effect on the catalytic performance of 7Cu-Ce/CeAl catalyst. With the help of Raman spectra, X-ray absorption spectroscopy, *in situ* diffuse reflectance infrared Fourier transform spectroscopy, *etc.*, it was clearly revealed that the abundant Cu^+/Ce^{3+} paired sites with surface synergetic oxygen vacancies (SSOV) on 7Cu-Ce/CeAl catalyst could effectively facilitate the adsorption and activation of CO and NO, thus significantly enhancing the NO removal efficiency.

1. Introduction

With the increase in vehicle ownership and the adoption of more stringent emission regulation worldwide, vehicle emission control has always been a key research area in response to the growing problem of air pollution [1]. Catalytic elimination was considered as the most efficient and cost-effective technology for vehicle emission control [2,3]. Carbon monoxide (CO), hydrocarbons (HCs) and nitrogen oxides (NO_x) are the most common harmful air pollutants emitted by vehicles. Aimed at the catalytic elimination of CO, HCs and NO, nowadays, three-way catalysts (TWC) are always placed as a key part in the gasoline vehicle exhaust treatment system [4]. One of the most important reactions taking place on TWC is the NO reduction by CO ($2NO + 2CO = N_2 + 2CO_2$), in which the catalytic elimination of NO and CO can be achieved simultaneously [5].

Noble metal catalysts, such as Rh, Pd and Pt catalysts supported on various supports, have been widely applied for NO + CO reaction [6–9]. However, the rising price of noble metals, especially Rh with the most excellent NO elimination performance and also the highest price ever, is driving the intensive search for alternative cost-effective catalysts [10]. According to our previous research, reducible metal oxides (*e.g.*, CuO_x, V_2O_5, CeO_2, MnO_x and SnO_x, *etc.*) could be used as important components within the catalysts for NO + CO reaction [11–16]. Moreover, it has been reported that the mixed oxides or solid solutions composed of two or more reducible metal oxides (such as CuO_x-MnO_x, FeO_x-CoO_x and CuO_x-V_2O_5) could serve as more efficient catalysts for NO reduction by CO [11–14,17–19]. The enhanced catalytic performance on those multi-component metal oxide catalysts was resulted from the formation of more surface oxygen vacancies and more facile redox cycle within the reducible metal cations such as $Fe^{3+} + Co^{2+} \leftrightarrow Fe^{2+} + Co^{3+}$, $Cu^{2+} + V^{4+} \leftrightarrow Cu^{+} + V^{5+}$ and so on [11,12,17]. On such mixed oxides/solid solution catalytic systems, the surface oxygen vacancies could activate the N—O bond efficiently and then promote the dissociation of NO, which could be the rate-determining step in NO + CO reaction [12,20,21].

* Corresponding authors.
E-mail addresses: gaofei@nju.edu.cn (F. Gao), fudong.liu@ucf.edu (F. Liu).
[1] These authors contributed equally to this work.

https://doi.org/10.1016/j.cej.2022.140807
Received 9 October 2022; Received in revised form 24 November 2022; Accepted 3 December 2022
Available online 6 December 2022

Meanwhile, the adsorbed CO would react with O species dissociated from N—O to complete the catalytic cycle. To reveal the promotion effect of bimetal cations in mixed oxides/solid solution catalysts for NO + CO reaction, previously, we proposed a new concept of surface synergetic oxygen vacancy (SSOV) on a $CuO/Mn_2O_3/Al_2O_3$ model catalyst, which was formed by the depletion of oxygen between Cu and Mn cations [14]. The paired cation sites and SSOV were considered as the core local structures for the construction of highly efficient metal oxide catalysts for NO + CO reaction.

CeO_2 based catalysts have been widely applied in environmental catalysis field due to their superior redox property, environmental friendliness and relatively low cost [22]. To further promote the redox property of CeO_2 and increase the concentration of surface oxygen vacancies, various strategies such as morphology/size control and doping/modifying CeO_2 with other metal cations (Sn^{4+}, Mn^{4+}, Cu^{2+}, *etc.*) have been developed [12,23–26]. Modifying CeO_2 with Cu species has been proven as an effective strategy to achieve these goals due to the easy formation of strong interaction between Cu species and CeO_2 [27,28]. Therefore, CuO-CeO_2 based materials can be potentially developed into highly active NO + CO catalysts for practical applications [16,29,30]. To further tap the potential of CuO-CeO_2 based catalysts in NO + CO reaction, it is necessary to develop new synthesis strategies to optimize the local structure of CuO-CeO_2 active sites for maximizing the synergistic effect between Cu species and CeO_2 and creating more surface oxygen vacancies. Recently, we developed a unique two-step incipient wetness impregnation (*T*-IWI) method to promote the dispersion of CeO_2 on commercially available γ-Al_2O_3, and the obtained small CeO_2 particles with rich surface oxygen vacancies could be used as superior supports for Pd and Pt targeting low temperature catalytic oxidation reactions [31–33]. In this study, by introducing CuO species onto this novel CeO_2-Al_2O_3 support in a proper way, the redox property of CeO_2-Al_2O_3 could be further promoted, and the obtained CuO/CeO_2-Al_2O_3 catalyst was proven to perform superior catalytic activity for NO + CO reaction (reductant rich condition), one of the most important reactions on TWC for the gasoline vehicle emission control. Through a series of characterizations and reaction mechanism study, a clear structure–activity relationship of the newly developed CuO/CeO_2-Al_2O_3 catalyst in NO reduction by CO was established.

2. Experimental

2.1. Catalyst preparation

The preparation of new CuO-CeO_2-Al_2O_3 catalysts started from the deposition of 10 wt% CeO_2 (using $Ce(NO_3)_3{\cdot}6H_2O$ as precursor) onto commercial γ-Al_2O_3 (provided by Sasol with surface area of 150 $m^2{\cdot}g^{-1}$) by a conventional incipient wetness impregnation (IWI) method, followed by calcination at 800 °C for 2 h. The obtained 10 wt% CeO_2/Al_2O_3 support was denoted as 10CeAl-800. Afterwards, a mixed solution of $Ce(NO_3)_3$ and $Cu(NO_3)_2$ was added dropwise onto 10CeAl-800 by IWI method (*i.e.*, co-IWI), leading to the loading of *x* wt% CuO (*x* = 5, 7, 10) and additional 20 wt% CeO_2. The final CuO-CeO_2/10CeAl-800 serial catalysts were calcined at 550 °C for 2 h and denoted as *x*Cu-Ce/CeAl (*x* equals weight percentage of CuO, and the total CeO_2 loading within catalysts was controlled at 30 wt%).

For comparison, CuO counterpart catalysts supported on 30 wt% CeO_2/Al_2O_3 (30CeAl) and γ-Al_2O_3 were also prepared by IWI method. To prepare 30CeAl, $Ce(NO_3)_2$ solution was impregnated onto γ-Al_2O_3 leading to 30 wt% CeO_2 loading, followed by calcination at 550 °C for 2 h. The loading of CuO on 30CeAl and γ-Al_2O_3 was controlled at 7 wt% based on the activity screening results for *x*Cu-Ce/CeAl serial catalysts (with 7 wt% CuO as optimal loading). After calcination at 550 °C for 2 h, two counterpart catalysts were obtained and denoted as 7Cu/CeAl and 7Cu/Al, respectively.

To evaluate the thermal stability of prepared catalysts, 7Cu-Ce/CeAl and 7Cu/CeAl were aged in air at 800 °C for 12 h or in reaction flow (1000 ppm NO + 2000 ppm CO + 5 vol% H_2O, He as balance) at 800 °C for 1 h. The aged samples were denoted as 7Cu-Ce/CeAl-A, 7Cu/CeAl-A, 7Cu-Ce/CeAl-AR and 7Cu/CeAl-AR (-A = Aged in air; -AR = Aged in reaction flow).

2.2. Catalytic activity measurement

Catalytic performance evaluation for NO reduction by CO was conducted on a fixed-bed quartz tube reactor under steady state conditions. The gas feed stream was composed of 2000 ppm CO, 1000 ppm NO, 5 vol % H_2O (when needed), 600 or 3200 ppm O_2 (when needed), and 600 ppm C_3H_6 (when needed), using He as balance. For each test, 30 mg of catalyst (40–60 mesh) was diluted with 300 mg SiC to minimize the heat effect. The total flow rate was controlled at 100 $mL{\cdot}min^{-1}$, thus giving a weight hourly space velocity (WHSV) of 200,000 $mL{\cdot}g_{cat}^{-1}{\cdot}h^{-1}$. An online gas chromatograph (GC) equipped with a thermal conduction detector (TCD) and a column packed with 5A and 13X molecular sieves was used to measure the concentration of NO, CO and N_2 in the outlet gas. The NO conversion and N_2 selectivity were calculated according to the following equations:

$$NO\ conversion\ (\%) = \left(\frac{[NO]_{in} - [NO]_{out}}{[NO]_{in}}\right) \times 100\%$$

$$N_2\ selectivity\ in\ NO + CO\ reaction\ (\%) = \left(\frac{2[N_2]_{out}}{[NO]_{in} - [NO]_{out}}\right) \times 100\%$$

2.3. Catalyst characterizations

Water contact angles on different samples were measured on an optical tensiometer (OneAttension, Kruss Scientific Instrument) using the sessile drop method.

X-ray powder diffraction (XRD) patterns were collected on a Thermo Fisher Scientific X'TRA diffractometer with Cu $K\alpha_1$ radiation source (0.15406 nm) under a voltage of 40 kV and a current of 40 mA. The XRD patterns were collected over a 2θ range of 15–85°. The scan step was 0.02° and the scan speed was $8^{o}{\cdot}min^{-1}$.

Specific surface areas of prepared samples were calculated from N_2 adsorption–desorption isotherms measured at −196 °C on a Micromeritics ASAP 2020 analyzer, using the Brunauer-Emmett-Teller (BET) method. Prior to each test, the sample was degassed at 300 °C in vacuum for 4 h.

Raman spectroscopy was measured on a Renishaw Invia Plus laser Raman spectrometer (Renishaw, UK), using an Ar^+ laser beam. The emission line was set at 532 nm and the laser power was 20 mW.

NO-temperature-programmed desorption (NO-TPD) experiment was performed on a fixed-bed quartz tube reactor, using an online mass spectrometer (MS) to monitor the signal of NO and N_2. The sample was pretreated at 200 °C for 1 h under Ar (50 $mL{\cdot}min^{-1}$) and then cooled to room temperature. Afterwards, the sample was exposed to a flow of 1% NO/Ar (50 $mL{\cdot}min^{-1}$) to saturation. Then, the Ar flow (50 $mL{\cdot}min^{-1}$) was switched on to remove the weakly adsorbed NO. Finally, the sample was heated from room temperature to 600 °C with a ramping rate of 10 $^{o}C{\cdot}min^{-1}$.

X-ray photoelectron spectroscopy (XPS) was measured on a Thermo Fisher ESCALAB Xi+ instrument equipped with an Al Kα source gun (1486.6 eV). The binding energies (BE) of all elements were calibrated with C1s at 284.6 eV.

X-ray absorption spectroscopy (XAS) for the Cu-K edge of synthesized catalysts was measured in fluorescence mode at 7-BM QAS beamline of the National Synchrotron Light Source II (NSLS-II) at Brookhaven National Laboratory. The XAS data including X-ray absorption near edge structure (XANES) and extended X-ray absorption fine structure (EXAFS) were analyzed using the Demeter software package. Cu foil reference was used for energy calibration and monochromator drift correction. For Fourier-transformed EXAFS spectra, the

k range between 2.0 and 11.0 $Å^{-1}$ was used, and the curve fitting in the R range for the first and second coordination shells was between 1.0 and 2.8 Å in Artemis software.

High-resolution transmission electron microscopy (HR-TEM) images were collected on a JEM-2100 instrument. The energy dispersive spectroscopy (EDS) elemental mapping images were collected from a JEOL 2100F microscope (200 kV) equipped with an EDX analysis system.

Electron paramagnetic resonance (EPR) experiments were performed on a Bruker EMX-10/12 X-band spectrometer, which was operated at a frequency of $\nu \approx 9.48$ GHz and 100 kHz field modulation. The spectra for all catalysts were recorded at 110 K.

H_2-temperature-programmed reduction (H_2-TPR) experiment was performed in a quartz U-tube reactor, using a TCD to monitor the signal of H_2. The samples were pretreated with purified air at 200 °C for 1 h and then cooled to room temperature. Then, the samples were exposed to a flow of 7% H_2/Ar (10 mL·min^{-1}) and heated from 40 to 900 °C with a ramping rate of 10 °C·min^{-1}.

In situ diffuse reflectance infrared Fourier transform spectroscopy (*in situ* DRIFTS) was performed on a Nicolet 5700 FT-IR spectrometer using an MCT detector. The spectra were collected from 400 to 4000 cm^{-1} at a spectral resolution of 4 cm^{-1} for 64 scans. Prior to each test, the sample was purged with purified air at 400 °C for 0.5 h. Then, the sample was cooled and kept at 225 °C at which the background spectrum was collected and subtracted from the recorded spectrum automatically. For *in situ* NO + CO adsorption/reaction experiments, the feeding gas (40 mL·min^{-1}) containing 5000 ppm CO (when used), and/or 2500 ppm NO (when used) in Ar was introduced into the gas cell. The DRIFTS data were presented in Kubelka-Munk function.

3. Results and discussion

3.1. Structural information

As we previously reported, through the deposition of 10 wt% CeO_2 followed by calcination at 800 °C for 2 h, the surface hydrophilicity of γ-Al_2O_3 could be greatly improved [31,32]. On such high-temperature pre-calcined CeO_2/Al_2O_3 support (10CeAl-800) with higher surface hydrophilicity, the adsorption and dispersion of subsequently impregnated precursor solution could be significantly promoted. The water contact angles on 10CeAl-800 and γ-Al_2O_3 supports were tested (**Fig. S1**). As expected, a much lower water contact angle was observed on 10CeAl-800 (18°) than on γ-Al_2O_3 (29°), suggesting that 10CeAl-800 indeed showed higher surface hydrophilicity than γ-Al_2O_3.

To investigate the dispersion of CeO_2 and/or CuO species loaded on γ-Al_2O_3, CeAl and 10CeAl-800 supports, the XRD patterns for 7Cu/Al, 7Cu/CeAl and *x*Cu-Ce/CeAl were collected. As shown in Fig. 1**a**, the diffraction peaks assigned to CeO_2 (JCPDS No. 34–0934) and γ-Al_2O_3 (JCPDS No. 50–0741) were observed on all CeO_2 and Al_2O_3 containing catalysts. For *x*Cu-Ce/CeAl catalysts, only when the CuO loading reached 10 wt%, the diffraction peaks assigned to crystalline CuO could be detected (JCPDS No. 44–0706). However, in contrast to 7Cu-Ce/CeAl with no CuO crystal phase, for 7Cu/Al and 7Cu/CeAl catalysts, the diffraction peaks assigned to crystalline CuO could be clearly observed, suggesting the higher dispersion of Cu species within 7Cu-Ce/CeAl. Moreover, the intensity of the diffraction peaks assigned to CeO_2 for 7Cu-Ce/CeAl was significantly lower than those for 7Cu/CeAl (Fig. 1**b**), which was due to the lower crystallinity of CeO_2 particles within 7Cu-Ce/CeAl. The relatively larger full width at half maximum (FWHM) of the XRD peak assigned to CeO_2(1 1 1) on 7Cu-Ce/CeAl (0.95°) comparing to that on 7Cu/CeAl (0.92°) further suggested that the 7Cu-Ce/CeAl catalyst showed lower CeO_2 crystalline size (9.4 nm) than 7Cu/CeAl (9.7 nm). The specific surface areas of the prepared catalysts were also measured (Table 1). Due to the use of the same γ-Al_2O_3 as base support, 7Cu/CeAl and 7Cu-Ce/CeAl catalysts showed no difference in the specific surface area.

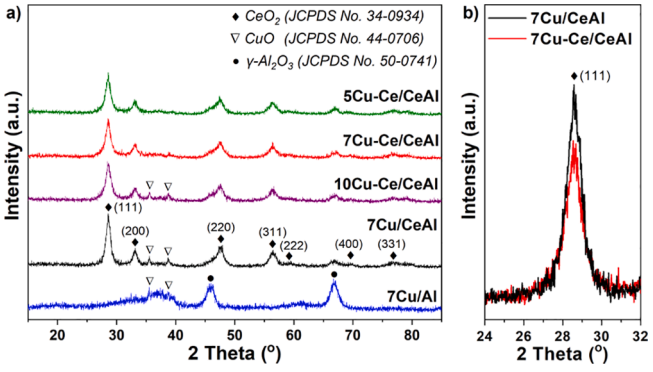

Fig. 1. a) XRD patterns for 7Cu/Al, 7Cu/CeAl and *x*Cu-Ce/CeAl serial catalysts; **b)** XRD patterns for 7Cu/CeAl and 7Cu-Ce/CeAl with a 2 Theta range of 24–32°.

HR-TEM images of 7Cu/CeAl and 7Cu-Ce/CeAl catalysts were collected to further elucidate their morphology and microstructure. As demonstrated in Fig. 2**a–d**, much smaller CeO_2 particles were observed on 7Cu-Ce/CeAl (*ca.* 20 nm) than on 7Cu/CeAl (*ca.* 100 nm), suggesting the higher dispersion of CeO_2 on 7Cu-Ce/CeAl catalyst due to the unique preparation method. Since it was difficult to distinguish Cu species and CeO_2 from HR-TEM images due to the low mass-thickness contrast, to investigate the dispersion state of Cu species, EDS mapping results for 7Cu/CeAl and 7Cu-Ce/CeAl were collected (Fig. 2**e, f**). It was found that the dispersion of Cu species on both catalysts mainly followed that of CeO_2 although a small portion of Cu was also present on Al_2O_3, which was due to the nature that Cu could interact with CeO_2 more preferentially than with γ-Al_2O_3.

3.2. Catalytic performance

The catalytic performance of *x*Cu-Ce/CeAl serial catalysts with CuO loading of 5, 7, and 10 wt% in NO + CO reaction was first evaluated (**Fig. S2**). When the CuO loading reached 7 wt%, 7Cu-Ce/CeAl catalyst exhibited the optimal NO reduction activity. As shown in Fig. 3**a**, comparing to 7Cu/CeAl and 7Cu/Al with 7 wt% CuO loading as well prepared by conventional IWI method, 7Cu-Ce/CeAl still performed the best among the three catalysts. A T_{50} (the temperature at which NO conversion reached 50%) of *ca.* 245 °C was achieved on 7Cu-Ce/CeAl, which was much lower than that on 7Cu/CeAl (*ca.* 300 °C) and 7Cu/Al (*ca.* 380 °C). 7Cu-Ce/CeAl also exhibited higher N_2 selectivity (> 95 %) than 7Cu/CeAl and 7Cu/Al counterparts (**Fig. S3**). The impact of O_2 and hydrocarbon on the catalytic performance of 7Cu-Ce/CeAl catalyst

Table 1
Data summary on specific surface area, Raman spectra and XPS analysis.

Samples	BET SA ($m^2·g^{-1}$) [a]	I_D/I_{F2g} (a.u.) [b]	Surface atomic concentration (%) [c]				$Ce^{3+}/(Ce^{3+}+Ce^{4+})$ (%) [d]
			Al	O	Ce	Cu	
7Cu/Al	116	–	40.0	58.1	–	1.9	–
7Cu/CeAl	86	0.22	39.4	57.8	0.8	2.0	14.3
7Cu-Ce/CeAl	86	0.78	39.0	57.4	1.3	2.4	18.6
30CeAl	101	–	36.3	62.5	1.2	–	14.1
10CeAl-800	90	–	38.7	60.7	0.6	–	28.8

[a] BET surface area determined by N_2 adsorption–desorption isotherms measured at −196 °C.
[b] The peak area ratio of D-band (I_D) and CeO_2 F_{2g} band (I_{F2g}) in Raman spectra.
[c] Surface atomic concentration determined by XPS analysis.
[d] Ce^{3+} ratio among total Ce species in each sample, which was calculated according to the formula: Ce^{3+} (%) = $(S_{v^0} + S_{v'} + S_{u^0} + S_{u'}) / \sum(S_v + S_u)$, where S_v and S_u were the areas of the peaks labeled as v and u, respectively, in Ce 3d XPS.

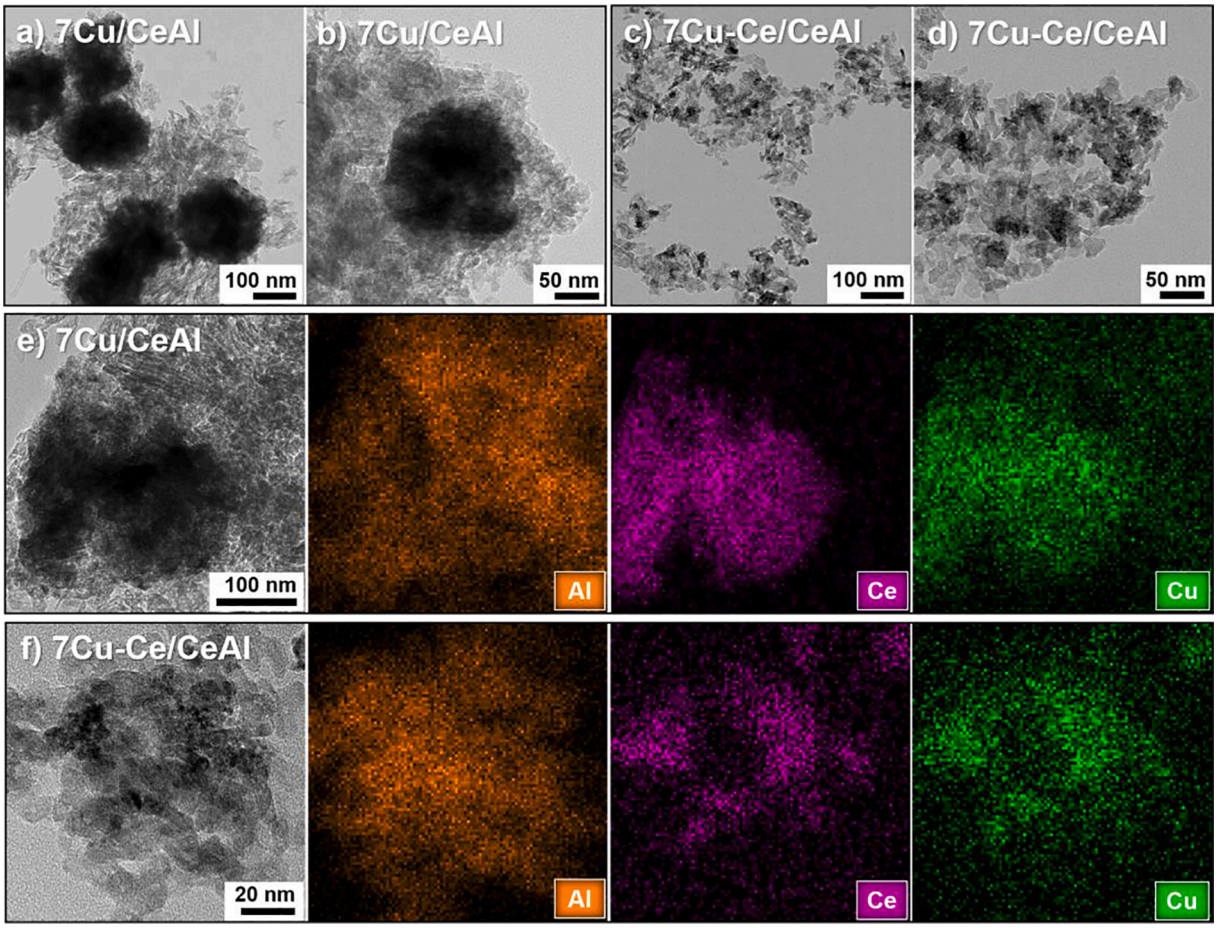

Fig. 2. HR-TEM images of **a, b)** 7Cu/CeAl and **c, d)** 7Cu-Ce/CeAl. EDS mapping results of **e)** 7Cu/CeAl and **f)** 7Cu-Ce/CeAl.

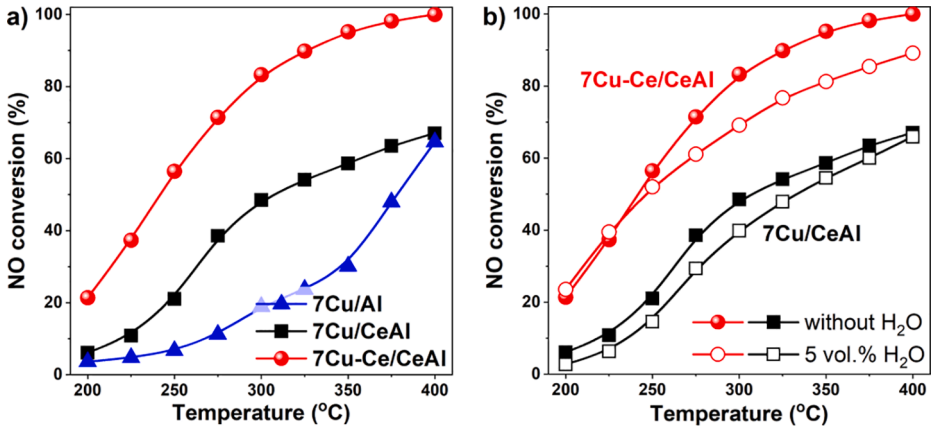

Fig. 3. **a)** NO + CO activity on 7Cu/Al, 7Cu/CeAl and 7Cu-Ce/CeAl; **b)** NO + CO activity on 7Cu/CeAl and 7Cu-Ce/CeAl in the presence of 5 vol% H_2O.

was also evaluated by adding O_2 and C_3H_6 to the feeding gas. As shown in Fig. S4, after the introduction of 600 ppm O_2, the NO conversion on 7Cu-Ce/CeAl decreased, which could be caused by the preferential reaction between CO and O_2. When C_3H_6 was also introduced (2000 ppm CO + 1000 ppm NO + 600 ppm C_3H_6 + 3200 ppm O_2, which a stoichiometric reaction condition), the NO removal efficiency on 7Cu-Ce/CeAl decreased significantly, suggesting that CO was consumed by O_2 at low temperatures ($\leq$ 200 °C) while C_3H_6 was not an ideal reductant to react with NO on CuO-CeO_2-Al_2O_3 catalysts.

For vehicle emission control catalysts, H_2O may have a dramatic impact on the catalytic performance due to the competitive adsorption with other reactants or the changing of reaction pathways [34]. Therefore, it is highly necessary to investigate the H_2O effect on the NO reduction performance for the CuO-CeO_2 catalysts developed in this work. With the introduction of 5 vol% H_2O to the reactant flow, no significant decrease in the NO reduction activity was observed on both 7Cu/CeAl and 7Cu-Ce/CeAl catalysts (Fig. 3**b**). 7Cu-Ce/CeAl still exhibited much higher NO removal efficiency than 7Cu/CeAl with H_2O present in the reaction stream. Moreover, the long-term activity evaluation at 300 °C in the presence of H_2O further revealed that 7Cu-Ce/CeAl showed superior stability under wet reaction condition (Fig. S5), indicating the high potential of the newly developed CuO-CeO_2-Al_2O_3

catalyst for practical application. Thermal stability was another key performance indicator of vehicle emission control catalysts. To evaluate the thermal stability of 7Cu-Ce/CeAl catalyst in comparison to 7Cu/CeAl, the NO + CO activity of the aged catalysts (under 800 °C in air condition for 12 h) was also tested (Fig. S6). Although both 7Cu-Ce/CeAl and 7Cu/CeAl suffered from the deactivation to a certain extent resulted from thermal aging, 7Cu-Ce/CeAl-A (-A = Aged in air) still performed higher NO reduction efficiency than 7Cu/CeAl-A. After the high temperature (800 °C) treatment in reaction flow (CO + NO + H_2O + He) for 1 h, 7Cu-Ce/CeAl-AR (-AR = Aged in reaction flow) still outperformed 7Cu/CeAl-AR, especially in the low temperature range (Fig. S7). Furthermore, during the cyclic activity test from 150 to 400 °C, the NO + CO activity on 7Cu-Ce/CeAl catalyst showed no decrease at all but even a slight increase after the first run (Fig. S8), suggesting the satisfactory catalytic stability of 7Cu-Ce/CeAl catalyst under real reaction atmosphere.

3.3. The status of Cu species

Surface oxygen vacancies have been considered playing an important role in the NO + CO reaction on metal oxide catalysts [14]. To characterize the surface oxygen vacancies on 7Cu-Ce/CeAl in comparison to 7Cu/CeAl, the Raman spectra were collected, normalized and demonstrated in Fig. 4**a**. The intensive band at *ca.* 457 cm^{-1} was ascribed to the triply degenerate F_{2g} mode of fluorite-type CeO_2 lattice, and the band at *ca.* 590 cm^{-1} could be assigned to oxygen defects (D-bands) [35,36]. Interestingly, the D-band on 7Cu-Ce/CeAl was much more intensive than that on 7Cu/CeAl, suggesting that more oxygen vacancies were formed on 7Cu-Ce/CeAl. The peak area ratio of D-band (I_D) to CeO_2 F_{2g} band (I_{F2g}), *i.e.,* I_D/I_{F2g}, could be used to indicate the relative concentration of oxygen defects on CeO_2 materials [24]. As listed in Table 1, much higher relative concentration of oxygen defects was indeed achieved on 7Cu-Ce/CeAl (0.78) than on 7Cu/CeAl (0.22). Since the oxygen defects could facilitate the activation/dissociation of NO [12], the higher concentration of surface oxygen defects on 7Cu-Ce/CeAl catalyst could be one of the main reasons for its higher NO + CO activity. The NO-TPD results further supported the viewpoint that the adsorbed NO on 7Cu-Ce/CeAl catalyst was much easier to decompose to N_2 than on 7Cu/CeAl counterpart (Fig. S9).

Besides the surface oxygen vacancies, the state of Cu species could also have a significant impact on the adsorption and activation of reactants. Although XRD and EDS mapping have shown that the Cu species on 7Cu-Ce/CeAl catalyst were in highly dispersed state, a clear understanding on the intrinsic nature of Cu species was still missing. As a powerful tool for characterizing the reducibility and elucidating the structure of CuO-CeO_2 catalysts, H_2-TPR experiments were conducted. As illustrated in Fig. 4**b**, Fig. S10 and Table S1, the broad H_2-consumption peak at 100–350 °C for CuO-CeO_2-Al_2O_3 catalysts was related to the reduction of CuO_x species and adjacent CeO_2. Moreover, this broad peak on 7Cu-Ce/CeAl and 7Cu/CeAl could be deconvoluted into three sub-peaks, correlating to different types of CuO_x species. For 7Cu/Al reference, the H_2-consumption peak could be deconvoluted into two sub-peaks (γ' and γ''), which could be assigned to the reduction of small CuO_x clusters and relatively larger CuO_x particles on pristine Al_2O_3 support, respectively. According to previous reports and the H_2-TPR profile for 7Cu/Al reference, peak α, peak β and peak γ on 7Cu/CeAl and 7Cu-Ce/CeAl could be attributed to highly dispersed CuO_x clusters, Cu-O-Ce structure (Cu ions incorporated into CeO_2 matrix, *i.e.*, Cu-O-Ce solid solution) and CuO_x clusters/particles on Al_2O_3 surface, respectively [37–40]. Not surprisingly, all the H_2-consumption sub-peaks on 7Cu-Ce/CeAl shifted to lower temperatures by *ca.* 25–40 °C comparing to those on 7Cu/CeAl, suggesting that much better redox property was achieved on the newly developed 7Cu-Ce/CeAl catalyst. Moreover, the peaks γ on 7Cu/CeAl and 7Cu-Ce/CeAl were located at similar temperatures as peak γ'' and peak γ' on 7Cu/Al, respectively, which suggested that the multistage co-IWI method could effectively facilitate the dispersion of CuO_x species, and only a small portion of CuO_x species within 7Cu-Ce/CeAl were deposited on Al_2O_3 surface as small CuO_x clusters. The H_2-consumption amount on 7Cu/CeAl and 7Cu-Ce/CeAl was also calculated and listed in Table S1 using CuO as standard sample. It was found that the total H_2-consumption amount (peak α + peak β + peak γ) on 7Cu/CeAl (1003 μmol·g^{-1}) and 7Cu-Ce/CeAl (1035 μmol·g^{-1}) was much higher than the theoretical value for the complete reduction of CuO to metallic Cu (875 μmol·g^{-1}), suggesting that some Ce^{4+} species adjacent to Cu species (*i.e.*, Cu-O-Ce structure, peak β) were also reduced due to the H_2-spillover effect. Furthermore, it is noteworthy that the peak α on 7Cu-Ce/CeAl was much more intensive than that on 7Cu/CeAl, indicating the formation of more highly dispersed CuO_x clusters within 7Cu-Ce/CeAl. It has been reported that the highly dispersed CuO_x species on CeO_2 based supports were highly efficient in CO oxidation and preferential oxidation (PROX) of CO in H_2 [41,42]. Over 7Cu-Ce/CeAl, the formation of more highly dispersed CuO_x clusters could play an important role in the adsorption and activation of CO for NO + CO reaction. Furthermore, the peak γ on 7Cu-Ce/CeAl was much weaker than that on 7Cu/CeAl, suggesting that much less crystalline CuO species were formed on 7Cu-Ce/CeAl than on 7Cu/CeAl, as verified by the previous XRD results.

EPR analysis was also conducted as supplementary evidence to determine the Cu speciation. As shown in Fig. 4**c, a** partially resolved A type signal with four line hyperfine splitting was observed on the EPR spectra for 7Cu/CeAl and 7Cu-Ce/CeAl, with $g_{||} = 2.327$, $A_{||} = 120$ G, and unresolved $g_\perp$ and $A_\perp$ parameters, which could be related to the isolated Cu^{2+} at octahedral sites in CeO_2 with a tetragonal distortion. Besides, a broad signal B with g = 2.155 and a signal K with g = 2.272 were observed, which could be assigned to the smaller CuO_x particles and the Cu^{2+} dimers in CeO_2 lattice, respectively [43,44]. It was also

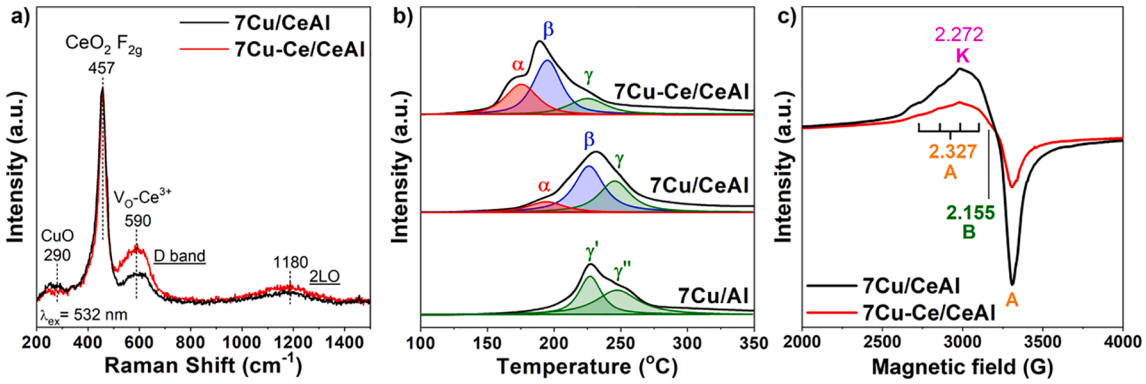

Fig. 4. a) Raman spectra for 7Cu/CeAl and 7Cu-Ce/CeAl catalysts. **b)** H_2-TPR profiles with deconvoluted sub-peaks for 7Cu/Al, 7Cu/CeAl and 7Cu-Ce/CeAl catalysts. **c)** EPR spectra for 7Cu/CeAl and 7Cu-Ce/CeAl catalysts.

found that the EPR signal of 7Cu/CeAl was much stronger than that of 7Cu-Ce/CeAl, suggesting the formation of more Cu^{2+} dimers and isolated Cu^{2+} ions on 7Cu/CeAl. Considering that limited amount of crystalline CuO was formed on 7Cu-Ce/CeAl in comparison to 7Cu/CeAl, the lower intensity of EPR signal for 7Cu-Ce/CeAl should be resulted from the highly dispersed CuO_x clusters with a dipolar broadening effect caused by the mutual interaction between neighboring paramagnetic Cu^{2+} ions [15]. In short summary, the EPR results further confirmed the viewpoint that more highly dispersed CuO_x clusters were formed on the new 7Cu-Ce/CeAl catalyst. Furthermore, although more isolated Cu species were formed on 7Cu/CeAl than on 7Cu-Ce/CeAl, much lower NO conversion was observed on 7Cu/CeAl, suggesting that the highly dispersed CuO_x clusters should be more active sites for NO reduction by CO, which was well supported by our previous work [43].

To obtain more information about Cu and Ce species, XPS was performed to measure the surface atomic concentration and probe the valence states of Cu and Ce on 7Cu/CeAl and 7Cu-Ce/CeAl. As listed in Table 1, higher concentration of surface Ce and Cu was observed on 7Cu-Ce/CeAl than on 7Cu/CeAl, due to the much smaller particle size of CeO_2 and higher dispersion of Cu species within 7Cu-Ce/CeAl catalyst resulted from the new preparation method. For the Cu 2p XPS of both 7Cu/CeAl and 7Cu-Ce/CeAl, three peaks at 933.8 (Cu $2p_{3/2}$), 953.4 (Cu $2p_{1/2}$) and 942.5 eV (shake up satellites) for characteristic Cu^{2+} species were observed (Fig. 5**a**), indicating that the Cu species within both catalysts were mainly in the form of Cu^{2+} [45].

As shown in Fig. 5**b**, Ce 3d XPS for 7Cu/CeAl and 7Cu-Ce/CeAl were deconvoluted into ten sub-peaks. The peaks labeled as u and v were attributed to the Ce $3d_{3/2}$ (u) and Ce $3d_{5/2}$ (v) contributions, respectively. The sub-peaks labeled as u^0, u', v^0 and v' were ascribed to the Ce^{3+} species while the others were assigned to the Ce^{4+} species. The concentration of surface Ce^{3+} was calculated and listed in Table 1 [38]. It was found that higher concentration of surface Ce^{3+} species (18.6%) was obtained on 7Cu-Ce/CeAl than on 7Cu/CeAl (14.3%). Combined with the HR-TEM, H_2-TPR and EPR results, it can be concluded that the smaller particle size of CeO_2 as well as the more abundant CuO_x clusters-CeO_2 interfaces on 7Cu-Ce/CeAl catalyst should account for its higher concentration of surface Ce^{3+} species. The Ce 3d XPS also well supported the Raman spectra results showing that more surface oxygen vacancies could be easily formed on 7Cu-Ce/CeAl, which was always closely related to the presence of more Ce^{3+} species. Under the real reaction condition, higher concentration of Ce^{3+} species could not only facilitate the formation of oxygen vacancies but also improve the redox property of Cu sites ($Cu^{2+} \leftrightarrow Cu^{+}$), which could be one of the reasons for higher reducibility of 7Cu-Ce/CeAl catalyst as indicated by H_2-TPR. Such synergistic effect between the oxygen vacancies and redox sites (Cu and Ce cations) could effectively enhance the NO activation, thus significantly promoting the catalytic performance of 7Cu-Ce/CeAl for NO reduction by CO.

XAS analysis was further conducted to help reveal the valence states and local coordination structure of Cu species. As illustrated in Fig. 5**c**, the white line intensity of Cu-K XANES for 7Cu/CeAl and 7Cu-Ce/CeAl catalysts were similar to those for CuO and $Cu(NO_3)_2$, indicating that the Cu species in both catalysts were in the form of Cu^{2+}, matching well with the Cu 2p XPS results (Fig. 5**a**). Moreover, according to the results of

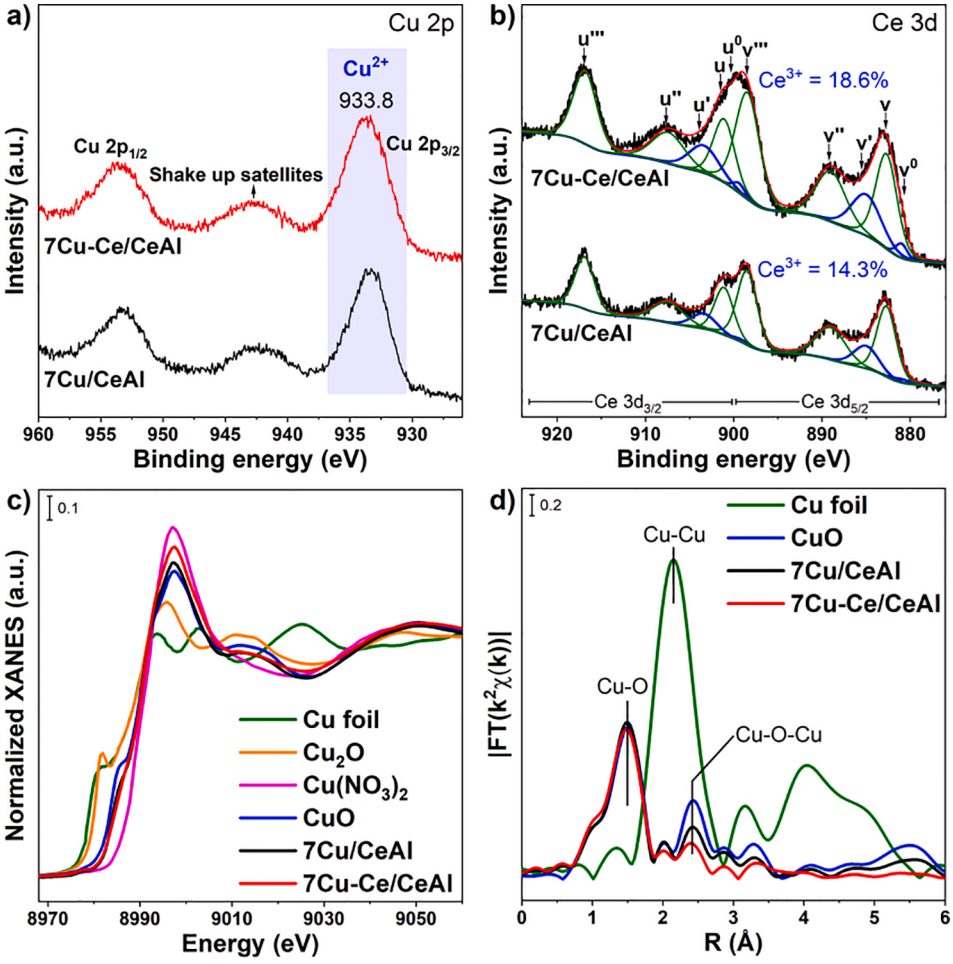

Fig. 5. a) Cu 2p and **b)** Ce 3d XPS for 7Cu/CeAl and 7Cu-Ce/CeAl catalysts. **c)** Normalized XANES and **d)** EXAFS of Fourier transformed k^2-weighted $\chi(k)$ at the Cu-K edge for 7Cu/CeAl and 7Cu-Ce/CeAl catalysts.

XANES linear combination fitting (Fig. S11, Table S2), the relatively more accurate valence states of Cu species on 7Cu/CeAl (1.90 ± 0.11) and 7Cu-Ce/CeAl (2.02 ± 0.11) were obtained. The slightly lower valence state of Cu species within 7Cu/CeAl catalyst could be due to the formation of larger CuO_x particles containing Cu^0 or Cu^+ species. To further investigate the local coordination structure of Cu species, EXAFS curve fitting analysis was conducted. As demonstrated in Fig. 5**d**, for both 7Cu/CeAl and 7Cu-Ce/CeAl catalysts, no Cu-Cu coordination shell was observed, indicating the absence of metallic Cu clusters or particles. The exclusive presence of Cu-O and Cu-O-Cu coordination shells suggested that the Cu species in both catalysts were in the form of isolated Cu^{2+} ions and/or CuO_x clusters/particles. According to the EXAFS fitting results (Fig. S12, Table S3), the coordination number (CN) of Cu-O-Cu on 7Cu-Ce/CeAl ($CN_{Cu\text{-}O\text{-}Cu} = 1.3 \pm 0.1$) was lower than that on 7Cu/CeAl ($CN_{Cu\text{-}O\text{-}Cu} = 2.1 \pm 0.2$), suggesting that the CuO_x clusters on 7Cu-Ce/CeAl should be smaller than those on 7Cu/CeAl. When combined with the results of Raman spectra, H_2-TPR, XPS, *etc.*, it can be concluded that a higher amount of smaller CuO_x clusters were formed on 7Cu-Ce/CeAl catalyst, thus generating more CuO_x-CeO_2 interfaces and surface oxygen vacancies. Such a unique local structure of 7Cu-Ce/CeAl catalyst could be the main reason for its higher NO + CO activity.

3.4. Reaction mechanism study

To further reveal the reasons for the superior NO + CO activity on 7Cu-Ce/CeAl and gain insight into the reaction mechanism, a systematic *in situ* DRIFTS study was performed. Since the Cu sites for CO adsorption and activation should be vital for NO + CO reaction, the *in situ* DRIFTS of CO adsorption was first conducted. As illustrated in Fig. 6**a**, the CO adsorption peak on 7Cu-Ce/CeAl at *ca.* 2101 cm^{-1} was much more intensive than that on 7Cu/CeAl, which was related to linear CO adsorbed on Cu^+ species (as Cu^{2+} could be reduced to Cu^+ in CO atmosphere at 225 °C) [41]. This result suggested that more exposed Cu sites with higher reducibility for CO adsorption and activation were successfully constructed on the newly developed 7Cu-Ce/CeAl catalyst.

In situ DRIFTS of NO adsorption on 7Cu/CeAl and 7Cu-Ce/CeAl was performed to investigate the nature of adsorbed NO species (Fig. 6**b**). On 7Cu/CeAl catalyst, the NO adsorption resulted in the obvious formation of monodentate nitrates located at 1300 and 1480–1530 cm^{-1}. Besides, two weak bands at *ca.* 1596 and 1611 cm^{-1} were also observed on 7Cu/CeAl, which could be assigned to bridging monodentate nitrates and bridging bidentate nitrates, respectively [14,18,46]. Comparatively, on 7Cu-Ce/CeAl catalyst, besides the observation of monodentate nitrates (1300 and 1480–1530 cm^{-1}), much more chelating bidentate nitrates (1250 and 1559 cm^{-1}) and linear nitrites (1277 cm^{-1}) were clearly observed [12,47], which might be related to the NO adsorbed on the sites adjacent to the rich CuO_x cluster-CeO_2 interfaces.

To evaluate the reactivity of CO adsorbed on Cu sites, *in situ* DRIFTS of NO reacting with pre-adsorbed CO (without cutting off the CO flow) was conducted (Fig. 7**a and b**). With the introduction of NO into the feed stream, the CO@Cu^+ bands at *ca.* 2100 cm^{-1} decreased significantly on both 7Cu-Ce/CeAl and 7Cu/CeAl catalysts. Simultaneously, the increment of gas phase CO_2 at 2300–2400 cm^{-1} was observed, suggesting

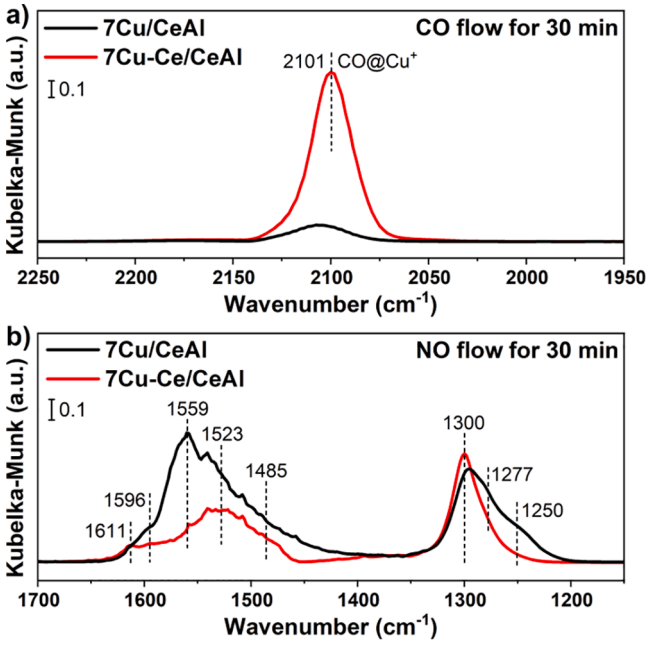

Fig. 6. *In situ* DRIFTS of **a)** CO adsorption and **b)** NO adsorption on 7Cu/CeAl and 7Cu-Ce/CeAl catalysts at 225 °C.

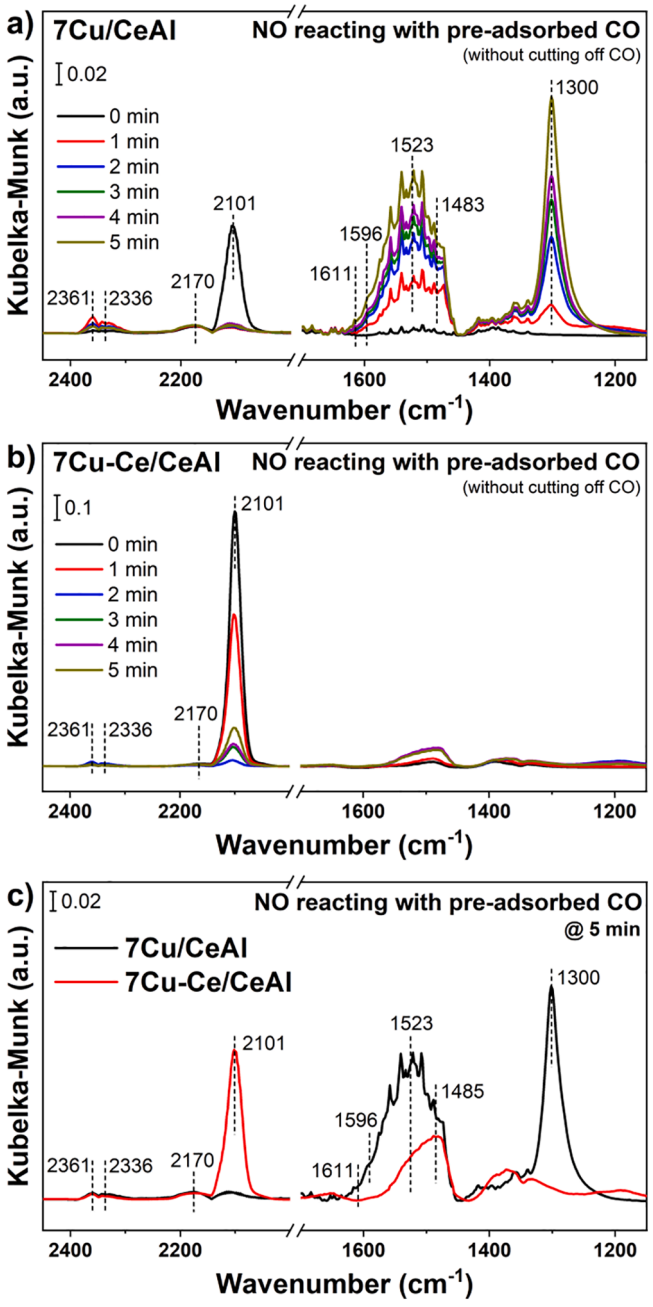

Fig. 7. *In situ* DRIFTS of NO reacting with pre-adsorbed CO on **a)** 7Cu/CeAl and **b)** 7Cu-Ce/CeAl at 225 °C; **c)** The selected DRIFTS spectra of NO reacting with pre-adsorbed CO on 7Cu/CeAl and 7Cu-Ce/CeAl catalysts at 225 °C for 5 min.

that the adsorbed CO on Cu^+ sites could react with NO rapidly at 225 °C. The maximum yield of CO_2 was achieved in the first 1–2 min, suggesting that the abundant surface oxygen vacancies generated by CO adsorption/reduction before the introduction of NO (CO + Cu^{2+}-[O]-Ce^{4+} → Cu^+-□-Ce^{3+} + CO_2, □ = surface oxygen vacancies) could better facilitate the dissociation of NO and the subsequent reaction between CO-Cu^+ and activated oxygen species. A similar process was also observed on Ru/CeO_2 catalyst that Ru^+-□-Ce^{3+} species played an important role in the activation of NO, as reported by Khivantsev *et al.* recently [48]. The generation of more Cu^+ sites and surface oxygen vacancies induced by the excess CO in the feeding gas could also well explain the improved NO removal efficiency on 7Cu-Ce/CeAl catalyst during the cyclic activity test (**Fig. S8**).

Meanwhile, although the resulting bands from NO adsorption on 7Cu-Ce/CeAl and 7Cu/CeAl showed comparable intensities (Fig. 6**b**), as clearly illustrated in Fig. 7**c**, much weaker bands assignable to adsorbed NO species were found on 7Cu-Ce/CeAl. Such results indicated that more efficient reaction between CO and NO could proceed on 7Cu-Ce/CeAl so that the surface coverage of adsorbed NO species was much lower on this new catalyst under the reaction condition. It is noticeable that almost no chelating bidentate nitrates and linear nitrites could be detected on 7Cu-Ce/CeAl, probably suggesting their higher reactivity in NO + CO reaction.

In situ DRIFTS of CO reacting with pre-adsorbed NO was conducted (with NO cut off) to further determine the reactivity of adsorbed NO species. As shown in Fig. 8**a**, on 7Cu/CeAl, monodentate nitrates (1300 and 1523 cm^{-1}), bridging monodentate nitrates (1596 cm^{-1}) and chelating bidentate nitrates (1250 and 1559 cm^{-1}) could be consumed by CO slowly. In clear contrast, once CO was introduced into the feed stream, the nitrate/nitrite species (including chelating bidentate nitrates at 1250 and 1559 cm^{-1}, and linear nitrites at 1277 cm^{-1}) on 7Cu-Ce/CeAl were consumed more rapidly within shorter period of time (Fig. 8**b**). These results indicated that the adsorbed NO species, particularly the abundant chelating bidentate nitrates and linear nitrites which probably mainly adsorbed at the CuO_x clusters-CeO_2 interface on 7Cu-Ce/CeAl catalyst, were highly reactive to the CO reductant.

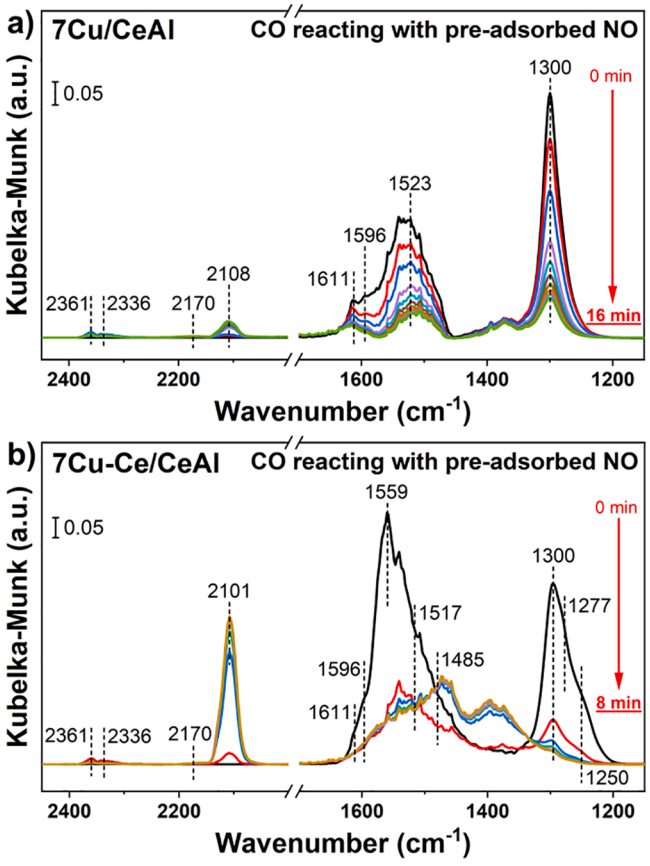

Fig. 8. *In situ* DRIFTS of CO reacting with pre-adsorbed NO on **a)** 7Cu/CeAl and **b)** 7Cu-Ce/CeAl catalysts at 225 °C.

Summarizing all the *in situ* DRIFTS results, it can be concluded that CO adsorbed on the highly dispersed CuO_x clusters could facilitate the reduction of Cu^{2+} species to reactive Cu^+ species and the generation of adjacent surface oxygen vacancies at CuO_x-CeO_2 interface. The surface oxygen vacancies could help the activation and dissociation of adsorbed NO, which could then rapidly react with highly reactive CO-Cu^+ and eventually generate N_2 and CO_2 as final products. Since 7Cu-Ce/CeAl catalyst possessed more highly dispersed CuO_x clusters with better redox property, more CuO_x clusters-CeO_2 interfaces and fruitful surface oxygen vacancies, the NO reduction by CO on 7Cu-Ce/CeAl catalyst could be dramatically boosted.

3.5. Discussion

For NO + CO reaction on metal oxide catalysts, the dissociation of NO is considered as the key step, and the surface oxygen vacancies near adsorbed NO species play a significant role in activating the N—O bond for further NO dissociation [14,17,21]. At the same time, the CO adsorbed on active sites adjacent to the oxygen vacancies can react with the surface oxygen atoms generated in NO dissociation to form CO_2, thus regenerating the oxygen vacancies [17,18]. The formation of catalytic domain (M_1^{p+}-□-M_2^{q+}, where -□- represents oxygen vacancy) with two redox sites (M_1^{p+}, M_2^{q+}) for NO and CO adsorption/activation as well as the surface synergetic oxygen vacancy (SSOV) can lead to excellent catalytic performance in NO reduction by CO [12,14].

According to the results of XRD, HR-TEM, EDS mapping, Raman spectroscopy, H_2-TPR and EPR, the microstructure of 7Cu/CeAl and 7Cu-Ce/CeAl catalysts can be clearly depicted. As shown in Fig. 9, the high-temperature pre-calcined 10CeAl-800 support with improved surface hydrophilicity could better facilitate the dispersion of CuO_x and CeO_2 at the same time within 7Cu-Ce/CeAl catalyst. More importantly, the higher dispersion of CeO_2 with smaller particle size could further promote the dispersion of CuO_x due to their higher concentration of surface defects and higher specific surface area. On 7Cu-Ce/CeAl catalyst, the bottom layer of CuO_x clusters and the Cu cations doped into CeO_2 matrix could drastically increase the concentration of oxygen vacancies on CeO_2 surface, especially at the CuO_x clusters-CeO_2 interface. As revealed by *in situ* DRIFTS results, such fine-tuned surface structure of 7Cu-Ce/CeAl catalyst could facilitate the efficient reduction of Cu^{2+} species to highly reactive Cu^+ species for CO adsorption/oxidation, and the nitrate/nitrite species adsorbed on 7Cu-Ce/CeAl were more reactive than those on 7Cu/CeAl. Accordingly, a scheme of NO + CO reaction mechanism on 7Cu-Ce/CeAl catalyst was also proposed and demonstrated in Fig. 9. The detailed reaction process can be described as follows:

CO + Cu^{2+}-[O]-Ce^{4+} → CO—Cu^{2+}-[O]-Ce^{4+} (1)

CO—Cu^{2+}-[O]-Ce^{4+} → Cu^+-□-Ce^{3+} + CO_2 (2)

CO + Cu^+-□-Ce^{3+} → CO—Cu^+-□-Ce^{3+} (3)

CO—Cu^+-□-Ce^{3+} + NO → CO—Cu^+-□-Ce^{3+}—NO (4)

CO—Cu^+-□-Ce^{3+}—NO → CO—Cu^{2+}-[O]-Ce^{4+}—[N] (5)

CO—Cu^{2+}-[O]-Ce^{4+}—[N] → Cu^+-□-Ce^{3+} + CO_2 + 1/2N_2(6)

When 7Cu-Ce/CeAl catalyst was exposed to NO + CO reaction flow, CO was mainly adsorbed on highly dispersed CuO_x clusters, and NO was preferentially adsorbed on Ce sites near the oxygen vacancies. The Cu^+-□-Ce^{3+} active sites could be formed *in situ* due to the facile reduction of Cu^{2+}-[O]-Ce^{4+} species by CO, which could effectively adsorb CO and

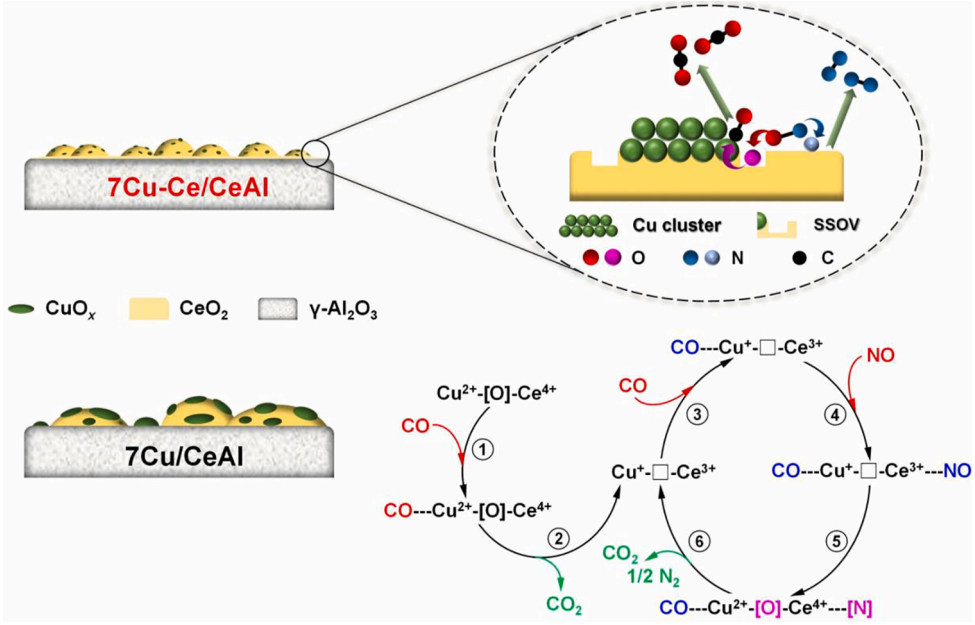

Fig. 9. The structural diagrams of 7Cu/CeAl and 7Cu-Ce/CeAl catalysts (left) and the scheme of reaction mechanism on 7Cu-Ce/CeAl (right).

catalyze the NO adsorption and dissociation. Then the dissociated [O] could be taken away by adsorbed CO to form CO_2, and the formed N radical ([N]) could combine with NO or another [N] to produce N_2O or N_2, respectively. At higher temperatures, the generation of N_2O could be decreased (as shown in Fig. S3), which should be due to the acceleration of [N] radical generation and subsequent coupling. Since more highly dispersed CuO_x clusters with superior redox property were formed on 7Cu-Ce/CeAl than on 7Cu/CeAl, more reactive Cu^+-□-Ce^{3+} sites could be created at the CuO_x clusters-CeO_2 interface under reaction condition, thus contributing to the much higher NO + CO activity on 7Cu-Ce/CeAl catalyst. In short summary, the *in situ* formed catalytic domain, Cu^+-□-Ce^{3+} species at the CuO_x clusters-CeO_2 interface, played a pivotal role in catalyzing the NO + CO reaction on CuO-CeO_2 based catalysts. This was mainly due to the synergistic effect between Cu^+ and Ce^{3+} as well as the assistance from the surface synergetic oxygen vacancy (SSOV). Comparing to the previous reports focusing on the interaction only between the two isolated redox sites, such SSOV concept was further extended to the clusters-support interfaces in this work.

4. Conclusions

Through a well-designed multistage co-IWI method, highly dispersed CuO_x clusters supported on smaller CeO_2 particles were successfully constructed on 7Cu-Ce/CeAl catalyst, which exhibited much more excellent activity, higher N_2 selectivity and superior stability in NO + CO reaction comparing to the 7Cu/Al and 7Cu/CeAl counterpart catalysts. 7Cu-Ce/CeAl also showed good resistance to H_2O poisoning which was beneficial for practical application. The catalytic domain of Cu^+-□-Ce^{3+} significantly contributed to the NO adsorption/dissociation and the oxidation of CO through a synergistic effect between Cu^+, Ce^{3+} and the surface synergetic oxygen vacancies (SSOV) at the CuO_x clusters-CeO_2 interfaces. The efficient catalytic cycle of NO adsorption/dissociation, oxygen transfer and CO oxidation achieved on 7Cu-Ce/CeAl catalyst was responsible for the boosted catalytic performance in NO reduction by CO. The simple synthesis route, low cost and superior catalytic performance have set this novel CuO-CeO_2-Al_2O_3 catalyst a highly promising candidate for vehicle emission control. The new insights into the SSOV concept from this work can provide solid theoretical guidance for the design of more efficient environmental catalysts for NO + CO reaction.

Declaration of Competing Interest

The authors declare that they have no known competing financial interests or personal relationships that could have appeared to influence the work reported in this paper.

Data availability

Data will be made available on request.

Acknowledgement

F. G. acknowledges the support from the National Natural Science Foundation of China (No. 21972063) and Natural Science Foundation of Jiangsu Province (BK20200012). F. L. acknowledges the Startup Fund from the University of Central Florida (UCF). S. X. thanks the support from the Preeminent Postdoctoral Program (P3) at UCF. F. L. sincerely thanks Dr. Marcos Schöneborn at Sasol for providing raw materials in catalyst synthesis. This research used beamline 7-BM (QAS) of the National Synchrotron Light Source II, a U.S. Department of Energy (DOE) Office of Science User Facility operated for the DOE Office of Science by Brookhaven National Laboratory under Contract No. DE-SC0012704.

Appendix A. Supplementary data

Supplementary data to this article can be found online at https://doi.org/10.1016/j.cej.2022.140807.

References

[1] A.K. Datye, M. Votsmeier, Opportunities and challenges in the development of advanced materials for emission control catalysts, Nat. Mater. 20 (2020) 1049–1059.
[2] H.S. Gandhi, G.W. Graham, R.W. McCabe, Automotive exhaust catalysis, J. Catal. 216 (2003) 433–442.
[3] R.J. Farrauto, M. Deeba, S. Alerasool, Gasoline automobile catalysis and its historical journey to cleaner air, Nat. Catal. 2 (2019) 603–613.
[4] C.K. Lambert, Current state of the art and future needs for automotive exhaust catalysis, Nat. Catal. 2 (2019) 554–557.
[5] P. Granger, V.I. Parvulescu, Catalytic NO_x abatement systems for mobile sources: from three-way to lean burn after-treatment technologies, Chem. Rev. 111 (2011) 3155–3207.
[6] P. Bera, K.C. Patil, V. Jayaram, G.N. Subbanna, M.S. Hegde, Ionic dispersion of Pt and Pd on CeO_2 by combustion method: Effect of metal-ceria interaction on

catalytic activities for NO reduction and CO and hydrocarbon oxidation, J. Catal. 196 (2000) 293–301.
[7] A. Buzková Arvajová, P. Boutikos, R. Pečinka, P. Kočí, Global kinetic model of NO oxidation on Pd/γ-Al_2O_3 catalyst including PdO_x formation and reduction by CO and C_3H_6, Appl. Catal. B 260 (2020), 118141.
[8] Z. Xu, Y. Li, Y. Lin, T. Zhu, A review of the catalysts used in the reduction of NO by CO for gas purification, Environ. Sci. Pollut. Res. 27 (2020) 6723–6748.
[9] K. Khivantsev, C.G. Vargas, J. Tian, L. Kovarik, N.R. Jaegers, J. Szanyi, Y. Wang, Economizing on precious metals in three-way catalysts: thermally stable and highly active single-atom rhodium on ceria for NO abatement under dry and industrially relevant conditions, Angew. Chem. Int. Ed. 60 (2021) 391–398.
[10] Price pressures on metals, Nat. Catal., 2 (2019) 735-735.
[11] Y. Xiong, X. Yao, C. Tang, L. Zhang, Y. Cao, Y. Deng, F. Gao, L. Dong, Effect of CO-pretreatment on the CuO-V_2O_5/γ-Al_2O_3 catalyst for NO reduction by CO, Catal. Sci. Technol. 4 (2014) 4416–4425.
[12] X. Yao, Y. Xiong, W. Zou, L. Zhang, S. Wu, X. Dong, F. Gao, Y. Deng, C. Tang, Z. Chen, L. Dong, Y. Chen, Correlation between the physicochemical properties and catalytic performances of $Ce_xSn_{1-x}O_2$ mixed oxides for NO reduction by CO, Appl. Catal. B 144 (2014) 152–165.
[13] X. Wang, Y. Lu, W. Tan, A. Liu, J. Ji, H. Wan, C. Sun, C. Tang, L. Dong, Insights into the precursor effect on the surface structure of γ-Al_2O_3 and NO + CO catalytic performance of CO-pretreated CuO/MnO_x/γ-Al_2O_3 catalysts, J. Colloid Interface Sci. 554 (2019) 611–618.
[14] D. Li, Q. Yu, S.-S. Li, H.-Q. Wan, L.-J. Liu, L. Qi, B. Liu, F. Gao, L. Dong, Y. Chen, The remarkable enhancement of CO-pretreated CuO-Mn_2O_3/γ-Al_2O_3 supported catalyst for the reduction of NO with CO: The formation of surface synergetic oxygen vacancy, Chem. Eur. J. 17 (2011) 5668–5679.
[15] J. Sun, C. Ge, X. Yao, W. Zou, X. Hong, C. Tang, L. Dong, Influence of different impregnation modes on the properties of CuO-CeO_2/γ-Al_2O_3 catalysts for NO reduction by CO, Appl. Surf. Sci. 426 (2017) 279–286.
[16] L. Liu, J. Cai, L. Qi, Q. Yu, K. Sun, B. Liu, F. Gao, L. Dong, Y. Chen, Influence of supports structure on the activity and adsorption behavior of copper-based catalysts for NO reduction, J. Mol. Catal. A: Chem. 327 (2010) 1–11.
[17] L. Wang, X. Cheng, Z. Wang, C. Ma, Y. Qin, Investigation on Fe-Co binary metal oxides supported on activated semi-coke for NO reduction by CO, Appl. Catal. B 201 (2017) 636–651.
[18] Y. Lv, L. Liu, H. Zhang, X. Yao, F. Gao, K. Yao, L. Dong, Y. Chen, Investigation of surface synergetic oxygen vacancy in CuO-CoO binary metal oxides supported on γ-Al_2O_3 for NO removal by CO, J. Colloid Interface Sci. 390 (2013) 158–169.
[19] X. Cheng, X. Zhang, D. Su, Z. Wang, J. Chang, C. Ma, NO reduction by CO over copper catalyst supported on mixed CeO_2 and Fe_2O_3: Catalyst design and activity test, Appl. Catal. B 239 (2018) 485–501.
[20] X. Yao, F. Gao, Q. Yu, L. Qi, C. Tang, L. Dong, Y. Chen, NO reduction by CO over CuO-CeO_2 catalysts: effect of preparation methods, Catal. Sci. Technol. 3 (2013) 1355–1366.
[21] A.G. Makeev, N.V. Peskov, The reduction of NO by CO under oxygen-rich conditions in a fixed-bed catalytic reactor: a mathematical model that can explain the peculiar behavior, Appl. Catal. B 132–133 (2013) 151–161.
[22] T. Montini, M. Melchionna, M. Monai, P. Fornasiero, Fundamentals and catalytic applications of CeO_2-based materials, Chem. Rev. 116 (2016) 5987–6041.
[23] Z. Su, W. Yang, C. Wang, S. Xiong, X. Cao, Y. Peng, W. Si, Y. Weng, M. Xue, J. Li, Roles of oxygen vacancies in the bulk and surface of CeO_2 for toluene catalytic combustion, Environ. Sci. Technol. 54 (2020) 12684–12692.
[24] W. Tan, J. Wang, L. Li, A. Liu, G. Song, K. Guo, Y. Luo, F. Liu, F. Gao, L. Dong, Gas phase sulfation of ceria-zirconia solid solutions for generating highly efficient and SO_2 resistant NH_3-SCR catalysts for NO removal, J. Hazard. Mater. 388 (2020), 121729.
[25] Z.-Y. Pu, X.-S. Liu, A.-P. Jia, Y.-L. Xie, J.-Q. Lu, M.-F. Luo, Enhanced activity for CO oxidation over Pr- and Cu-doped CeO_2 catalysts: effect of oxygen vacancies, J. Phys. Chem. C 112 (2008) 15045–15051.
[26] W. Tan, H. Alsenani, S. Xie, Y. Cai, P. Xu, A. Liu, J. Ji, F. Gao, L. Dong, E. Chukwu, M. Yang, F. Liu, Tuning single-atom Pt_1-CeO_2 catalyst for efficient CO and C_3H_6 oxidation: size effect of ceria on Pt structural evolution, ChemNanoMat 6 (2020) 1797–1805.
[27] P. Zhao, X. Li, W. Liao, Y. Wang, J. Chen, J. Lu, M. Luo, Understanding the role of NbO_x on Pt/Al_2O_3 for effective catalytic propane oxidation, Ind. Eng. Chem. Res. 58 (2019) 21945–21952.
[28] X. Wang, J.A. Rodriguez, J.C. Hanson, D. Gamarra, A. Martínez-Arias, M. Fernández-García, In situ studies of the active sites for the water gas shift reaction over Cu-CeO_2 catalysts: Complex interaction between metallic copper and oxygen vacancies of ceria, J. Phys. Chem. B 110 (2006) 428–434.
[29] P. Bera, S.T. Aruna, K.C. Patil, M.S. Hegde, Studies on Cu/CeO_2: a new NO reduction Catalyst, J. Catal. 186 (1999) 36–44.
[30] Y. Hu, L. Dong, M. Shen, D. Liu, J. Wang, W. Ding, Y. Chen, Influence of supports on the activities of copper oxide species in the low-temperature NO+CO reaction, Appl. Catal. B 31 (2001) 61–69.
[31] S. Xie, Z. Wang, W. Tan, Y. Zhu, S. Collier, L. Ma, S.N. Ehrlich, P. Xu, Y. Yan, T. Xu, J. Deng, F. Liu, Highly active and stable palladium catalysts on novel ceria-alumina supports for efficient oxidation of carbon monoxide and hydrocarbons, Environ. Sci. Technol. 55 (2021) 7624–7633.
[32] W. Tan, S. Xie, X. Wang, C. Wang, Y. Li, T.E. Shaw, L. Ma, S.N. Ehrlich, A. Liu, J. Ji, F. Gao, L. Dong, F. Liu, Highly efficient Pt catalyst on newly designed CeO_2-ZrO_2-Al_2O_3 support for catalytic removal of pollutants from vehicle exhaust, Chem. Eng. J. 131855 (2021).
[33] S. Xie, W. Tan, C. Wang, H. Arandiyan, M. Garbrecht, L. Ma, S.N. Ehrlich, P. Xu, Y. Li, Y. Zhang, S. Collier, J. Deng, F. Liu, Structure-activity relationship of Pt catalyst on engineered ceria-alumina support for CO oxidation, J. Catal. 405 (2022) 236–248.
[34] R.H. Nibbelke, M.A.J. Campman, J.H.B.J. Hoebink, G.B. Marin, Kinetic study of the CO oxidation over Pt/γ-Al_2O_3 and Pt/Rh/CeO_2/γ-Al_2O_3 in the presence of H_2O and CO_2, J. Catal. 171 (1997) 358–373.
[35] W. Tan, J. Wang, S. Yu, A. Liu, L. Li, K. Guo, Y. Luo, S. Xie, F. Gao, F. Liu, L. Dong, Morphology-sensitive sulfation effect on ceria catalysts for NH_3-SCR, Top. Catal. 63 (2020) 932–943.
[36] S. Loridant, Raman spectroscopy as a powerful tool to characterize ceria-based catalysts, Catal. Today 373 (2021) 98–111.
[37] C. Wang, X.-K. Gu, H. Yan, Y. Lin, J. Li, D. Liu, W.-X. Li, J. Lu, Water-mediated Mars-van Krevelen mechanism for CO oxidation on ceria-supported single-atom Pt_1 catalyst, ACS Catal. 7 (2017) 887–891.
[38] L. Qi, Q. Yu, Y. Dai, C. Tang, L. Liu, H. Zhang, F. Gao, L. Dong, Y. Chen, Influence of cerium precursors on the structure and reducibility of mesoporous CuO-CeO_2 catalysts for CO oxidation, Appl. Catal. B 119–120 (2012) 308–320.
[39] M.-F. Luo, J.-M. Ma, J.-Q. Lu, Y.-P. Song, Y.-J. Wang, High-surface area CuO-CeO_2 catalysts prepared by a surfactant-templated method for low-temperature CO oxidation, J. Catal. 246 (2007) 52–59.
[40] A. Chen, X. Yu, Y. Zhou, S. Miao, Y. Li, S. Kuld, J. Sehested, J. Liu, T. Aoki, S. Hong, M.F. Camellone, S. Fabris, J. Ning, C. Jin, C. Yang, A. Nefedov, C. Wöll, Y. Wang, W. Shen, Structure of the catalytically active copper-ceria interfacial perimeter, Nat. Catal. 2 (2019) 334–341.
[41] W.-W. Wang, W.-Z. Yu, P.-P. Du, H. Xu, Z. Jin, R. Si, C. Ma, S. Shi, C.-J. Jia, C.-H. Yan, Crystal plane effect of ceria on supported copper oxide cluster catalyst for CO oxidation: importance of metal-support interaction, ACS Catal. 7 (2017) 1313–1329.
[42] Y. Liu, Q. Fu, M.F. Stephanopoulos, Preferential oxidation of CO in H_2 over CuO-CeO_2 catalysts, Catal. Today 93–95 (2004) 241–246.
[43] A. Liu, L. Liu, Y. Cao, J. Wang, R. Si, F. Gao, L. Dong, Controlling dynamic structural transformation of atomically dispersed CuO_x species and influence on their catalytic performances, ACS Catal. 9 (2019) 9840–9851.
[44] J. Chen, Y. Zhan, J. Zhu, C. Chen, X. Lin, Q. Zheng, The synergetic mechanism between copper species and ceria in NO abatement over Cu/CeO_2 catalysts, Appl. Catal. A 377 (2010) 121–127.
[45] Y.A. May, W.-W. Wang, H. Yan, S. Wei, C.-J. Jia, Insights into facet-dependent reactivity of CuO-CeO_2 nanocubes and nanorods as catalysts for CO oxidation reaction, Chin. J. Catal. 41 (2020) 1017–1027.
[46] T. Boningari, S.M. Pavani, P.R. Ettireddy, S.S.C. Chuang, P.G. Smirniotis, Mechanistic investigations on NO reduction with CO over Mn/TiO_2 catalyst at low temperatures, Mol. Catal. 451 (2018) 33–42.
[47] X. Yao, Q. Yu, Z. Ji, Y. Lv, Y. Cao, C. Tang, F. Gao, L. Dong, Y. Chen, A comparative study of different doped metal cations on the reduction, adsorption and activity of CuO/$Ce_{0.67}M_{0.33}O_2$ (M = Zr^{4+}, Sn^{4+}, Ti^{4+}) catalysts for NO + CO reaction, Appl. Catal. B 130–131 (2013) 293–304.
[48] K. Khivantsev, N.R. Jaegers, H.A. Aleksandrov, L. Kovarik, M. Engelhard, I. Song, J. Tian, L. Chen, D. Meira, X.I.P. Hernandez, Identification of single Ru (II) ions on ceria as a highly active catalyst for abatement of NO_x pollutants. ChemRxiv. Cambridge: Cambridge Open Engage; 2022; This content is a preprint and has not been peer-reviewed. DOI: 10.26434/chemrxiv-2021-vr21g-v3.